Biosensors and Bioelectronics: X 14 (2023) 100343

Contents lists available at ScienceDirect

Biosensors and Bioelectronics: X

journal homepage: www.journals.elsevier.com/biosensors-and-bioelectronics-x

Mixed reality-integrated soft wearable biosensing glove for manipulating objects

Jihoon Kim [a,b,1], Allison Bayro [c,1], Jaeho Lee [a,b], Ira Soltis [a,b], Myunghee Kim [d], Heejin Jeong [c,e,*], Woon-Hong Yeo [a,b,f,g,**]

[a] George W. Woodruff School of Mechanical Engineering, Georgia Institute of Technology, Atlanta, GA, 30332, USA
[b] IEN Center for Human-Centric Interfaces and Engineering, Institute for Electronics and Nanotechnology, Georgia Institute of Technology, Atlanta, GA, 30332, USA
[c] School of Biological and Health Systems Engineering, Ira A. Fulton Schools of Engineering, Arizona State University, Tempe, AZ, 85287, USA
[d] Department of Mechanical and Industrial Engineering, The University of Illinois at Chicago, Chicago, IL, 60607, USA
[e] The Polytechnic School, Ira A. Fulton Schools of Engineering, Arizona State University, Mesa, AZ, 85212, USA
[f] Wallace H. Coulter Department of Biomedical Engineering, Georgia Institute of Technology and Emory University School of Medicine, Atlanta, GA, 30332, USA
[g] Parker H. Petit Institute for Bioengineering and Biosciences, Institute for Materials, Neural Engineering Center, and Institute for Robotics and Intelligent Machines, Georgia Institute of Technology, Atlanta, GA, 30332, USA

ARTICLE INFO

Keywords:
Mixed reality
Biosensing glove
Soft wearables
Object manipulation

ABSTRACT

Recent advances in flexible sensors and wireless electronics have driven the development of lightweight and ergonomic wearable sensing gloves. Such gloves can be employed in mixed reality (MR) environments to give haptic capabilities during interactions with various objects. However, no prior study shows a quantitative measurement of physical user interactions of object manipulation in MR. Here, we report an MR-integrated soft bioelectronic system on a glove for quantifying the changes in the user's pinching tasks. We use nano-manufacturing techniques to fabricate flexible sensors, wireless circuits, and stretchable interconnectors seamlessly integrated with a wearable glove. The wearable biosensing glove with an integrated capacitive pressure sensor evaluates how users interact directly and indirectly interact with objects. The direct mode describes a user's direct touching and manipulating objects in MR. In contrast, in the indirect mode, objects are located far away and touched via a narrow light beam. The virtual object measurement parameters include mass, movement latency, dynamic friction coefficient, angular drag coefficient, and linear drag coefficient. The experimental results with human subjects show positive, linear relationships between pinching force and dynamic friction coefficient and mass parameters during the direct manipulation mode. Collectively, the MR-enabled wearable biosensing glove system offers unique advantages in detecting physical interactions and sensory feedback for various rehabilitation applications and MR human-machine interfaces.

1. Introduction

Mixed reality (MR) interfaces allow users to combine virtual and real information. Namely, MR headsets such as the HoloLens 2 display virtual information to the human senses while users interact with the real world (Lopes et al., 2018). Many industries also integrate various sensors within MR peripherals to quantify human motions and cognitive states (Bannach et al., 2007; Spain et al., 2022). One integration of these sensors is within wearable sensing gloves (WSG), where the kinematics of the hands are quantified. Within the domain of MR applications, WSGs have been used for a variety of applications, including training (Muangpoon et al., 2020; Tsai et al., 2021), motion decoding (Cha et al., 2017; Dwivedi et al., 2020; Jiang et al., 2018), and rehabilitation (Alexandre et al., 2019; Wu et al., 2019). Specifically, several of these works integrate force sensors on the fingertips of a WSG for pinch detection (Almeida et al., 2019; Cappello et al., 2018). The pinching or

Abbreviations: MR, mixed reality; PCB, printed circuit board; PI, polyimide; PDMS, polydimethylsiloxane.

* Corresponding author. The Polytechnic School, Ira A. Fulton Schools of Engineering, Arizona State University, Mesa, AZ, 85212, USA.
** Corresponding author. George W. Woodruff School of Mechanical Engineering, IEN Center for Human-Centric Interfaces, Engineering, Georgia Institute of Technology, Atlanta, GA, 30332, USA.
E-mail addresses: heejin.jeong@asu.edu (H. Jeong), whyeo@gatech.edu (W.-H. Yeo).
[1] Equally contributed to this work.

https://doi.org/10.1016/j.biosx.2023.100343
Received 29 December 2022; Received in revised form 12 March 2023; Accepted 17 March 2023
Available online 24 March 2023

air bloom gesture is a common motion in MR environments for object interaction (Hamacher et al., 2016). Users open and close their first finger, thumb (pinching), or whole hand (air bloom) to signify an object selection. This gesture can be performed directly, where the virtual object is directly connected with the user's hand, or indirectly, where a ray is cast out from the hand to an object far away. In either case, once the user has made a direct or indirect connection with the virtual object, the pinching gesture enables selection and further rotation or translation. Furthermore, the objects within the MR environment have parameters that can be set to change the type of interaction that the user experiences. For example, physics parameters such as linear drag coefficient, angular drag coefficient, dynamic friction coefficient, mass, and movement latency are specified in MR application development programs such as Unity and augment the user interaction with the virtual object.

Rehabilitation is an area that has been primarily impacted by advances in MR application development and, precisely, object parameters (Jeong et al., 2022). Neurological disorders are the main reason for disability worldwide, with stroke being the leading cause (Feigin et al., 2020). There were 33 million stroke survivors alone in 2010 (an 84% increase over 20 years), indicating the dire necessity to improve rehabilitation processes (Shi et al., 2019). Movement impairment conditions such as stroke and Parkinson's disease can affect a patient's quality of life. They cannot participate in society to the degree they once could, are at high risk for comorbidity of depression and anxiety and represent an excessive burden on healthcare resources in the United States (Anderson et al., 2007; Brocklehurst et al., 1981). Traditionally, motor impairment following neurological injury and disorder is treated with physical therapy. A trainer manually guides the patient's body through exercises and judges their progress based on fitness tests. Prior works have evaluated the effects of different physical object parameters used in rehabilitation, such as mass (Cappello et al., 2018; Gailey et al., 2017), shape (Gailey et al., 2017), and surface finishes (Cappello et al., 2018) to augment the forces produced by the hand. Unfortunately, there are several shortcomings with traditional physical therapy protocols. First, it can be difficult for the patient to complete training repetitions with consistency and accuracy due to the manual guidance. Additionally, the feedback and analysis from training often feature limited quantitative data (Lünenburger et al., 2007). Finally, there is a significant dependence on the trainer to support the patient throughout long-term rehabilitation. Physical therapy progress can be hugely dependent on the expertise of the trainer. As a result, researchers are turning to MR to address these challenges in traditional rehabilitation procedures. One of these interactions is pinching force, which is critical for assessing a patient's rehabilitation progress in gripping tasks and upper-body mobility. A complete quantitative analysis of pinching force in MR systems has not yet been reported. Furthermore, there has been limited research that investigates how virtual object parameters augment pinching force.

This paper presents a soft wearable biosensing platform that is integrated with a glove, including pressure sensors, stretchable interconnectors, and flexible wireless electronics. This wearable system offers a complete quantitative analysis of pinching force in MR environments. We investigate the relationship between pinching force and various virtual object parameters, including dynamic friction coefficient, linear drag coefficient, angular drag coefficient, mass, and movement latency, in a series of ten custom Microsoft HoloLens applications. We also study the pinching force for both direct and indirect manipulation types. The MR-enabled wearable biosensing glove allows pinching force information to be quantitively captured during various object manipulation tasks. We experimentally validate the mechanical durability and electronic stability of the glove. The implication of this work provides detailed insight into the pinching force trends associated with varying object physics parameters and manipulation types. The result of this novel investigation offers direction for future work in optimizing patient rehabilitation outcomes during MR object manipulation.

2. Materials and methods

2.1. Fabrication of biosensing gloves

This study involves developing a biosensing glove with multiple electronic components, flexible circuits that enable wireless transmission, stretchable interconnects, and pressure sensors. The flexible printed circuit board (fPCB) provides enough flexibility to endure resistance change and stress concentration from placing on the back of the hand. The fPCB has a size of 25 mm by 30 mm and has 1.5 mm of thickness along with 4 discrete sections, capacitance to digital converter, voltage converter, microprocessor, and antenna. The circuit is powered by a lithium-ion battery (3.7 V, 40mhA, 1.13 g) which provides 3.7 V then the circuit transforms into the operational voltage of 3.0 V through voltage converter (S1318A30, ABLIC). The microprocessor (NRF52832, Nordic) read the digital value converted from capacitance to digital converter (FDC1004, Texas Instruments) and transforms the data into wirelessly deliverable form via Bluetooth low energy antenna. Further board information can be found in Fig. S1, along with details with lists of functional components and circuits.

2.2. Fabrication of pressure sensors

A glass slide is sprayed with release agent (Ease Release™, Smooth-On) to effectively remove the PDMS layer. Well-mixed 1:10 ratio polydimethylsiloxane (PDMS, Sylgard 184, Dow) is spin-coated (SCS 6800, KISCO) at 1500 rpm for 60 s and cured at 150 °C for 10 min. After cure, a 6 μm (BR0214, MSE Supplies) is layered on top of PDMS. The copper layer is laser fabricated with 5 mm × 8 mm flag pattern via high precision micro-laser processor (Femtosecond Laser Micro-Machining System, OPTEC). PDMS with 10:1 ratio is re-deposited as dielectric middle layer with 150 μm thickness by spin-coating at 500 rpm then patterned with just enough power to process through PDMS layer only while not ablating the copper layer. A 12 μm PI film (30HN Dupont™ Kapton®, Dupont) is covered on top to separate upper and bottom copper layer preventing shortage followed by upper copper film on top. The outline of sensors is processed with micro-laser processor then transferred to a new glass slide for encapsulation. The encapsulation of pressure sensor is done with PDMS again, fixing the structure and providing mechanical stability to be put on top of fingertip. Detailed schematics of the circuit and pressure sensor preparation are illustrated in Fig. S2.

2.3. Calibration of force-sensing gloves

To relate the measured capacitance (pF) from the pressure sensors to force measurements (N), a calibration is performed on each sensor prior to experimentation. A force gauge (Mark-10 Series 5) is used to apply incremental forces on the pressure sensors (Fig. S3A). The corresponding capacitance is observed and used to create a calibration curve. The derived linear equation is used to determine force measurements based on the pressure sensor capacitance values during the pinching gesture in MR (Fig. S3B).

2.4. Battery lifetime

The battery assembly with a magnetic charging port can be charged with 12 V–5 V converting circuit board connected by USB type-A and USB type-C. A Magnetic Switch is attached to control power status of the biosensing glove to easily turn on the device. A fully charged battery can power the glove over 25 h of continuous operation without disconnection, shown in Fig. S4, with only about 30 min of charging required.

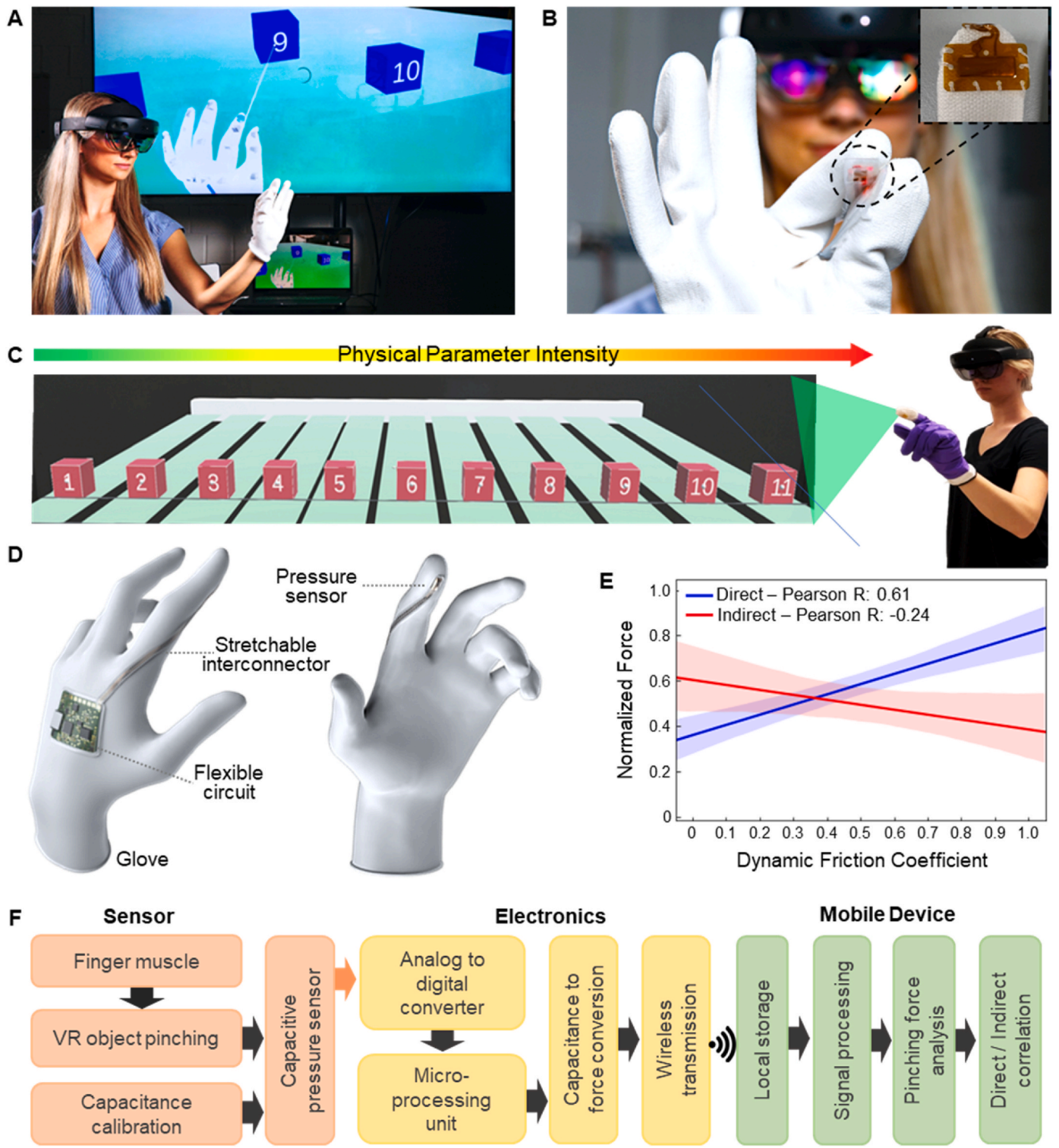

Fig. 1. Overview of an MR-enabled soft wearable biosensing glove for manipulating objects. (**A**) Photo of a user wearing a glove with MR goggles while MR projected view is shown on the rear screen. (**B**) Zoomed-in view of the pinching-detecting glove. (**C**) Illustration of MR view during pinching measure study where physical parameter intensity increases respectively. (**D**) Rendered frontal and backside view of pinching measure gloves with their component description. (**E**) Results of the pinching measure study showing the trend as dynamic friction coefficient changes. (**F**) Flowchart of the biosensing glove and MR system for data gathering, processing, and analyzing.

2.5. Processing of force sensor data

To process the force sensor data, a bandpass filter at 0.001 Hz–1 Hz was initially applied to remove the drift and offset value. From this, the absolute value of the signal was taken to correct for picofarad values that became negative from the initial bandpass filter (Fig. S5). Finally, a peak finding algorithm was applied to find the maximum capacitance value during each object interaction. In the case where the subject tried to manipulate a single cube more than one time, the largest peak was retained. To convert the information from the capacitive force sensor

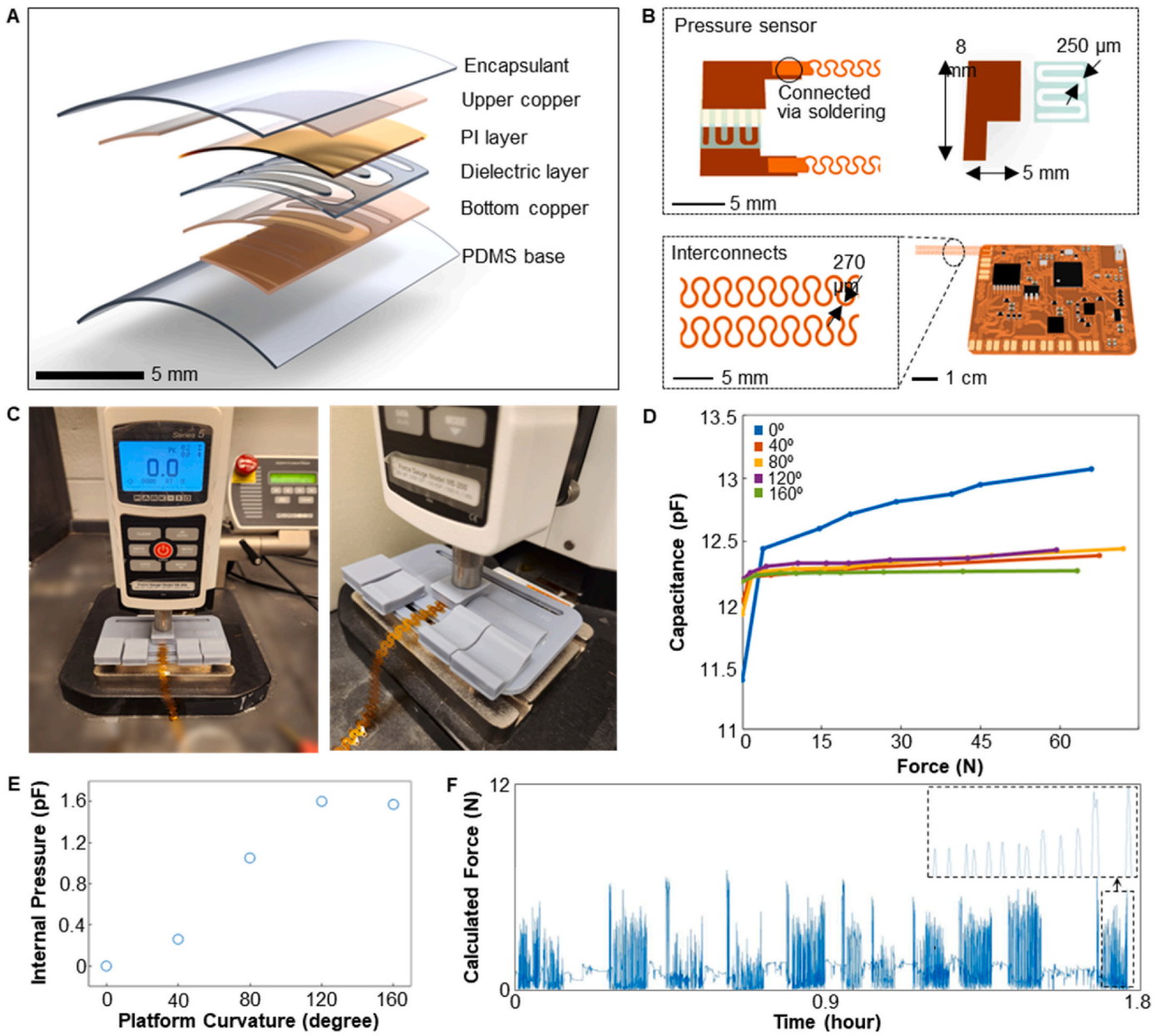

Fig. 2. Development of soft pressure sensors and interconnectors. (**A**) Illustration of pressure sensor structure array used in pinching force glove. (**B**) Details of the pressure sensor and interconnects with connection to fPCB. (**C**) Photos of pressure sensor calibration and mechanical test setup using a force transducer (left) with a zoomed-in view with curvature surface (right). (**D**) Calibration result of pressure sensor on surfaces with 0°, 40°, 80°, 120°, and 160° curvature. (**E**) Comparison of pre-loaded internal pressure due to platform curvature on different angles. (**F**) Result of hour-long sample session doing AR study tasks with pinching force glove. Inset shows a single task with detected pinching.

from picofarads to Newtons, we used the equation obtained from the pre-experimental calibration curve. The values for the force measurements were normalized to each subject by using the maximum pinching force value during the experiment.

2.6. Study procedures with human subjects

Five participants participated in this study. Most subjects reported moderate familiarity and experience with MR technologies, while only one had no prior familiarity or experience. The Institutional Review Board approved the experiment protocol (IRB #2021–0808) at the University of Illinois at Chicago. The subjects first completed a consent form and demographic survey. Following this, the subjects watched an instruction video on manipulation types. Then the subjects put on the HoloLens 2 MR headset and completed a practice session, which allowed them to manipulate objects directly and indirectly. Next, the subjects watched another instructional video and completed a second practice session teaching them how to perform several different types of object manipulations, such as sliding, rotating, and throwing in the MR applications. The practice session was a custom environment containing blocks with no varying physics parameters but contained the same setup as the experimental applications. After this, the subjects put on the novel pressure sensing glove and completed the same practice session to ensure correct fit and comfort during manipulation. Finally, the subjects completed the 10 mixed reality applications in a randomized order with 1-min rests in between. Prior to the experimental session, the subjects were told what type of manipulation (direct or indirect) will be used and the task to perform (e.g., throwing, sliding, rotating). In the direct mode, participants controlled the virtual object while having it physically attached to their hand. On the other hand, in the indirect mode, the

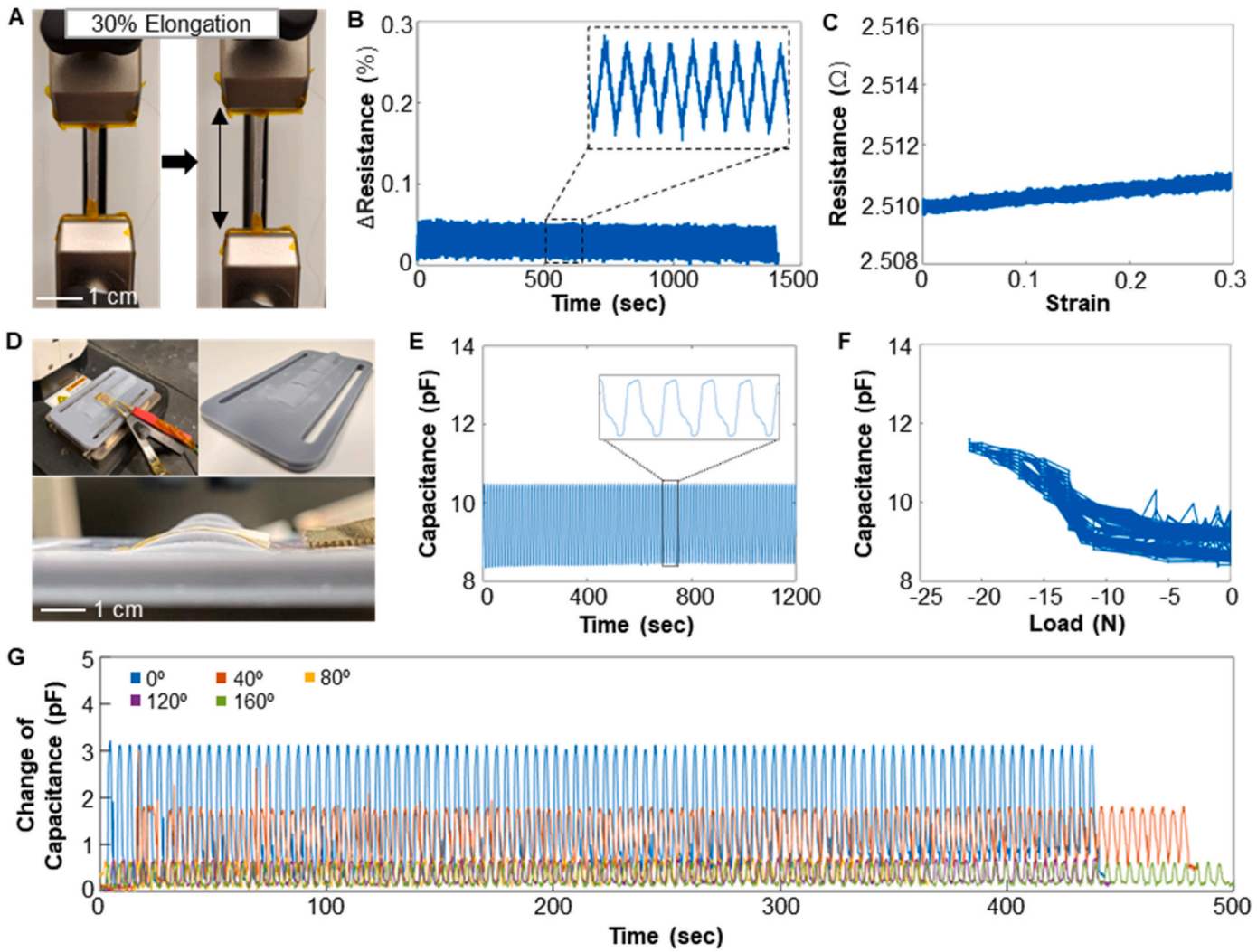

Fig. 3. Details of pressure sensor glove mechanical characterization. (**A**) Photos of pinching force glove interconnect elongation test setup on force transducer (left) with 30% strain (right). (**B**) Percent resistance change of the interconnectors in a mechanical test for 100 cycles of 30% elongation. (**C**) Changes of resistance during cyclic loading against 30% strain showing unified response. (**D**) Photos of pressure sensor cyclic loading on curvature platform (left), 3-D printed curvature platform (right), and side view of the pressure sensor for cyclic loading test (bottom). (**E**) Capacitance fluctuation under cyclic load for 100 cycles. (**F**) Changed of capacitance of a pressure sensor against a load up to 20 N for 100 cycles. (**G**) Capacitance fluctuation under cyclic loading for 100 cycles with various curvature platforms with 0°, 40°, 80°, 120°, and 160°.

participants used a hand ray to control distant virtual objects. The subjects were given 3 attempts per cube to complete the respective task before moving on. The number of attempts was selected based on previous testing of the application to ensure that participants could augment their object interaction in the case of a movement error (e.g., dropping the cube). For example, if the subjects could not slide the first cube to the finish line, they were allowed two more chances to bring the cube back to the beginning line and try again. This was incorporated to ensure that if the subject accidently dropped the cube during manipulation, they were given another opportunity to perform the task correctly.

3. Results and discussion

3.1. Overview of an MR-enabled soft biosensing glove system

To effectively quantify the subject's pinching force in real-time during given tasks, this study configures a flexible pinching force glove and a wearable headset (HoloLens2) that portrays MR. Fig. 1 represents the overview of the pinching force quantifying study with various in-app parameters. Fig. 1A pictures the subject wearing a mixed reality headset and biosensing glove while the subject's perspective is portrayed back screen. Fig. 1B shows a zoomed-in view of the biosensing system with a pinching motion. An example perspective of a given task, sliding a red block to the bolded line, is presented in Fig. 1C where each number on the block represents the parameter intensity increase respectively. The frontal and backside view of a biosensing glove with its component description is rendered in Fig. 1D, where the glove consists of five major parts: the pressure sensor, stretchable interconnect, flexible PCB, Battery assembly, and nylon glove. Fig. 1E delivers the relationship between the dynamic friction coefficient and normalized force on the task comparing direct and indirect pinching conditions. Direct pinching resulted in a Pearson correlation coefficient of 0.61, which is considered a strong relationship. However, indirect pinching resulted in −0.24, showing little correlation between the dynamic friction coefficient and pinching force. Fig. 1F illustrates a flowchart of how the biosensing system measures pinching force from the pressure sensor in real-time and flexible electronics transfers into a mobile device for post-measure analysis.

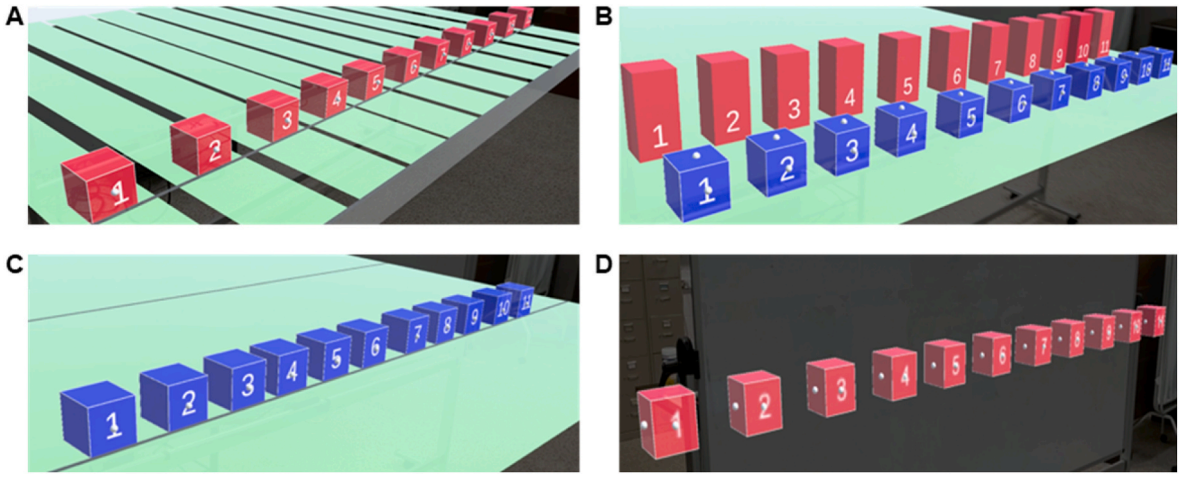

Fig. 4. Design of MR user interfaces with different pinching tasks. (**A**) Sliding of each red block from starting line to the endpoint (dynamic friction coefficient). (**B**) Stacking of the blue blocks on top of the corresponding red blocks (movement latency) or pushing over the red blocks with the corresponding blue blocks (mass). (**C**) Holding of the blue block in the air to throw it across the finishing line (linear drag coefficient). (**D**) Rotating of each red block with a single touch (angular drag coefficient). (For interpretation of the references to colour in this figure legend, the reader is referred to the Web version of this article.)

3.2. Development of soft pressure sensors and interconnectors

In Fig. 2, the design of a capacitive pressure sensor and its calibration is presented. Fig. 2A illustrates the capacitive pressure sensor structure array used in the wearable glove. The detailed dimensions of the fabricated pressure sensor are shown in Fig. 2B where the pressure sensor has a 5 mm × 5 mm main two metal platform with a 150 μm silicone dielectric layer in the middle. Stretchable interconnects are fabricated separately by micro-processing 6 μm copper film with a 270 μm width serpentine pattern. After the flexible circuit is prepared and the microprocessor is flashed with the corresponding software, the interconnect is soldered to connect the circuit and pressure sensor. The entire system is encapsulated before being put on a nylon glove with a biocompatible soft elastomer (Ecoflex™ 30, Smooth-On) support layer. While attaching the sensing system to the glove, another type of biocompatible soft elastomer is used with higher adhesion (Ecoflex™ Gel, Smooth-On) and provides a barrier layer to reduce stress concentration from curvature. Fig. 2C pictures the calibration setup used to test individual pressure sensors. This step is required to see the response and quality of the fabricated sensor and compare the result between the fabricated sensors to see the uniformity of fabrication because sensor fabrication has a high portion of human interaction. To consider the curvature of a human finger, a model platform is designed and printed with 3D printer ranging 0–160° with 40° increments having 2 cm × 2 cm base. The calibration in various curvature platforms has resulted in Fig. 2D where the 0-degree platform shows linear response and converges after 40 N with a slope of 0.035 pF/N; however, the curved platform drastically reduces sensitivity. Once placed on a curved surface, the differences in sensitivity change are not significant among the curved platform, 40-degree, 80-degree, and 120-degree curved platforms resulted in similar responses with a slope of 0.0083 pF/N. Still, the 160-degree platform showed minimal response total capacitance change of 0.1 pF in 60-N force. This is due to pre-loaded internal pressure when the pressure sensor is placed on a curved platform where the air movement inside the capacitive pressure sensor is more restricted as the surface curvature increases, which causes a reduction in pressure sensitivity (Fig. 2E). This trend of increasing internal capacitance due to curvature shows directly in the 0 force data in Fig. 2D, where the initial capacitance of the pressure sensor increases as internal pressure accumulates. A similar trend is also observed on a pressure sensor with a thinner dielectric layer. Fig. S6 portrays the initial capacitance difference due to internal stress when the sensors are attached to a curved surface. To validate the fabricated pressure sensor, an example task is made to demonstrate the system's functionality, shown in Fig. 2F. Each peak represents the detection of pinching with its magnitude calculated.

3.3. Mechanical characterization of sensors and interconnectors

Considering the study protocol, which requires multiple repetitions of pinching and hands gesturing more than hundreds of times, the mechanical stability and durability of the system must be approved before integrating it into the final design. The pressure sensor and stretchable interconnect are characterized by measuring their capacitance and resistance change, respectively. As shown in Fig. 3A, interconnects can stretch 30% from their original dimension vertically, exceeding human skin's physiological stretchability. An interconnector sample is prepared in the same condition it is used on the glove, with both edges exposed and soldered with copper wire to measure resistance. During the elongation test, each edge of interconnect is clipped on a force transducer (Motorized Force Gauge, Mark-10), with its resistance measured with a digital multimeter (DMM 7510, Keithley Instruments). The graph in Fig. 3B results from the change of resistance after 100 cycles of elongation in that there is less than 0.1% of total resistance change along the cyclic loading with little to no long-term shifts. Few loading cycles are detailed with zoomed-in view, showing uniform sinusoidal response. Fig. 3C shows the total resistance change against 100 cycles of strain with uniform and negligible response ranging between 2.51 Ω and 2.514 Ω. Detailed photos of the 3D printed platform and zoomed-in view are presented in Fig. 3D, along with a side view of how the pressure sensor is placed on top of the platform. To test the durability of the pressure sensor, another cyclic loading test has been made with the 0 N–25 N range on angled platforms (Radwin et al., 1992). A graph in Fig. 3E demonstrates the capacitance change of the pressure sensor during 100 cycles of pressurization. The pressure sensor retains distinct detection capability in the 0–5 N range. This result can be further mitigated with the difference between actual tasks and the testing environment where the cyclic loading is performed with an extreme case scenario involving a high volume repetition of more than 15 hard pinching in a minute. Additionally, Figs. S7–S8 show multiple tests proving additional stability and durability against 5 N and 50 N cyclic loads. The capacitance change uniformity of the pressure sensor against step loading is graphed in Fig. 3F showing a slow ramping response between 0 N and 10 N, a linear response between 10 N and 20 N, and convergence afterward. Overall, the graph shows minimal outliers in very low-pressure stages and negligible differences when the load exceeds 5 N ranging from 8.4 pF to 11.7 pF. A single-loop graph of the

Table 1
Performance comparison between this work and prior articles handling objects.

Reference	Form Factor	Sensor Type	Object Handling	Number of Gestures	Measured Physical Parameter					Application
					Mass	DFC	ADC	LDC	ML	
This work	Wireless gloves and soft electronics	Capacitive pressure sensor	Direct and Indirect	10	Yes	Yes	Yes	Yes	Yes	MR-based pinching force augmentation by varying physic parameters
(Tsai et al., 2021)	Wired gloves	Resistive force sensor	Direct only	1	Yes	–	–	–	–	VR-based baseball pitch training
(Dwivedi et al., 2020)	Wired gloves and wired sensors	Motion capture	Direct only	3	–	–	–	–	–	VR-based object motion decoding
(Muangpoon et al., 2020)	Wired sensors	Magnetic positioning	Direct only	1	–	–	–	–	–	AR-based rectal examination training
(Alexandre et al., 2019)	Wired gloves	Piezoresistive force sensor	Direct only	3	–	–	–	–	–	VR-based upper limb physical rehabilitation
(Almeida et al., 2019)	Wired sensors and wireless gloves	Piezoresistive force sensor	Direct only	4	–	–	–	–	–	VR-based increased immersion
(Cappello et al., 2018)	Robotic gloves	Gauge pressure sensor	Direct only	3	Yes	Yes	–	–	–	Assistive hand control
(Kim et al., 2021)	VR controller	Impedance transmission	Direct only	1	–	–	–	–	–	VR-based pinch detection
(Jiang et al., 2018)	Wired wristband	Motion capture	Direct only	6	–	–	–	–	–	VR-based hand grasp recognition and classification
(Cha et al., 2017)	Wired glove and wristband	Flexible piezoelectric sensor	Direct only	3	–	–	–	–	–	VR-based hand gesture recognition and classification
(Gailey et al., 2017)	Robotic gloves	Electromyogram sensor	Direct only	4	Yes	–	–	–	–	Prosthetic hand grasp assistance

DFC: dynamic friction coefficient.
ADC: angular drag coefficient.
LDC: linear drag coefficient.
ML: movement latency.

Table 2
Details of MR environment information for pinching tasks.

Physical Parameter	Range	Step	Task	Corresponding MR application in figures
Dynamic friction coefficient	0–1	0.1	Slide each cube from starting line to the ending line	Fig. 4A
Mass	1–100 kg	10 kg	Stack the blue cube on the red cube	Fig. 4B
Movement latency	0–0.5 s	0.05 s	Knock over the red cube of variable mass using the blue cube of constant mass (5 kg)	Fig. 4B
Linear drag coefficient	0–10	1	Throw each blue cube from starting line to the finish line	Fig. 4C
Angular drag coefficient	0–5	0.5	Rotate each free-floating cube one full revolution	Fig. 4D

load-capacitance curve is shown in Fig. S9. To further analyze the impact of the angled surface on pre-loaded pressure on the sensor, the cyclic loading test for 100 cycles is executed for all angled platforms, as shown in Fig. 3G. Following the results of the calibration stage, the sensitivity decreased as the curvature increased from the three pF range to 0.5 pF. Further curved surface cyclic loading details are shown in Fig. S10 with individual curvature-capacitance graphs.

3.4. Design of MR user interfaces and pinching tasks

The overview of a design MR user interface to manipulate multiple objects appears in Fig. 4. The MR applications supported on the HoloLens 2 are developed on Unity using the mixed reality toolkit. Each application is designed to have 11 cubes labeled 1–11 from left to right with an increasing physics parameter (i.e., movement latency, linear drag coefficient, dynamic friction coefficient, mass, and angular drag coefficient). Table 1 summarizes the comparison of the performance of the MR-enabled biosensing glove with other devices. A total of ten MR applications are individually developed for the experimental protocol. Namely, five physics parameters are studied: movement latency, linear drag coefficient, dynamic friction coefficient, mass, and angular drag coefficient. Two applications for direct and indirect manipulation are created for each of these five physics parameters. The range and step increase of the physics parameters are chosen based on shared values in literature and experimental pilot studies (Table 2). Furthermore, the Supplementary Videos S1–S5 exemplify the ten MR applications from the first and third-person perspectives. For the dynamic friction coefficient application, the effect that subjects feel is a change in the dynamic friction coefficient, which ultimately slows the sliding movement of the cube. The range of values is 0–1, with steps of 0.1 for each of the 11 cubes. The task for this application is to slide each block from the starting line to the finish line. The subject experienced surface resistance while sliding as the dynamic friction coefficient increased (Fig. 4A). For the mass application, the effect subjects feel is a change in mass, which ultimately makes the cubes feel heavier. The range of values is 1–100 kg with steps of 10 for each of the 11 cubes. The task for this application is to use a blue block with a constant mass of 1 kg to knock down red blocks of increasing mass. The subject experienced difficulty knocking down red blocks of larger mass (Fig. 4B). For the movement latency application, the effect subjects feel is a change in latency between the hand and cube movement. The range of values is 0–0.5 s with steps of 0.05 s for each of the 11 cubes. The task for this application is to stack the blue block on top of the red block. The subjects experienced a lag in the block movement while lifting and stacking as the latency increased (Fig. 4B). For the linear drag coefficient application, the effect subjects feel is a change in the linear drag coefficient, which ultimately slows the cube's movement. The range of values is 0–10, with steps of 1 for each of the 11 cubes. The task for this application is to throw each blue block from the starting line to the finish line. The subject experienced linear resistance while throwing as the linear drag coefficient increased (Fig. 4C). For the angular drag coefficient application, the effect subjects feel is a change in the angular drag coefficient, which ultimately slowed the rotational movement of the cube. The range of values is 0–5, with steps of 0.5 for each of the 11 cubes. The task for this application is to rotate the cubes one complete revolution with a single spin. The subject experienced

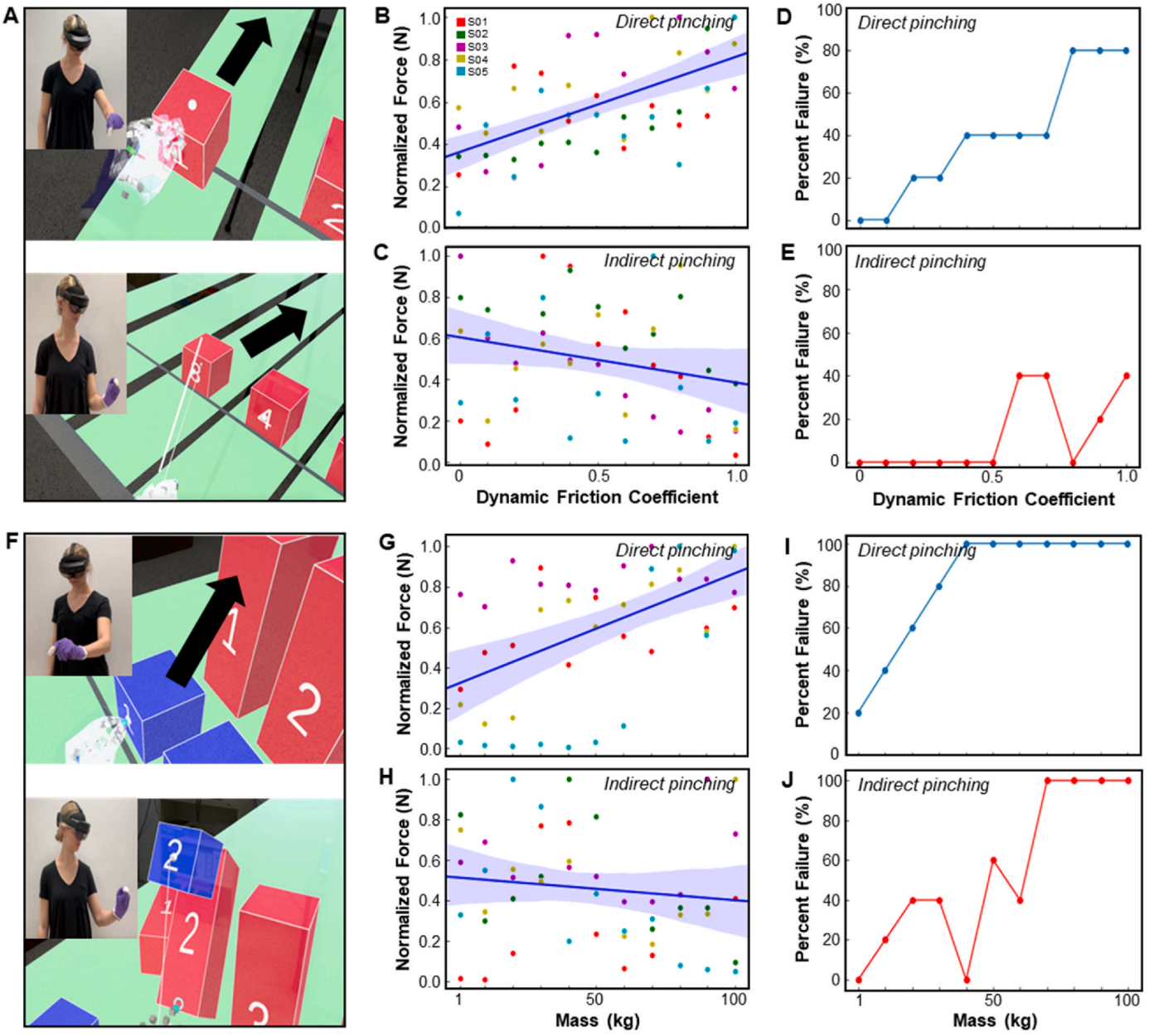

Fig. 5. Results of pinching force measurements with a biosensing glove in MR environments. (**A**) Photos of the subject's MR view using the pinching measure glove utilizing direct pinching (top) and indirect pinching (bottom) on changing dynamic friction coefficients. (**B**) Normalized pinching force according to dynamic friction coefficient when utilizing direct pinching (Pearson R: 0.61). (**C**) Normalized pinching force according to dynamic friction coefficient when utilizing indirect pinching (Pearson R: -0.24). (**D**) Failure trend of dynamic friction coefficient task with direct pinching. (**E**) Failure trend of dynamic friction coefficient task with indirect pinching. (**F**) Photos of the subject's MR view on changing mass when utilizing direct pinching (top) and indirect pinching (bottom). (**G**) Normalized pinching force according to increased mass utilizing direct pinching (Pearson R: 0.53). (**H**) Normalized pinching force according to increased mass utilizing indirect pinching (Pearson R: -0.13). (**I**) Failure trend of mass task with direct pinching. (**J**) Failure trend of mass task with indirect pinching.

angular resistance while spinning as the angular drag coefficient increased (Fig. 4D).

3.5. Results of pinching force measurements with a biosensing glove

The results of the pinching pressure measurement during the MR applications with increasing physics parameters show a positive linear trend during most direct manipulation interactions and no trend for indirect manipulation type. Specifically, the two highest direct manipulation correlations are compared to the corresponding indirect manipulation in Fig. 5. The first- and third-person viewpoint of the dynamic friction coefficient direct and indirect MR application is portrayed in Fig. 5A. The normalized pinching force results for five subjects during direct manipulation of MR object with increasing dynamic friction coefficient shows a strong (Mukaka 2012) positive linear relationship ($r = 0.61$, $p < 0.001$; Fig. 5B). Comparatively, the indirect manipulation type for this application shows no correlation with increasing dynamic friction coefficient parameters ($r = -0.24$, $p > 0.05$; Fig. 5C). The percent failure rate further supports these findings during the MR application, which is defined as the number of subjects who could not complete the manipulation task of the cube divided by the total number of subjects. Fig. 5D shows an increasing percent failure for direct manipulation where the sliding task was successful for the first two dynamic friction coefficients for all subjects and unsuccessful for all

Table 3
Correlation coefficients for direct and indirect pinching applications.

Physical Parameter	Correlation Coefficient	
	Direct Manipulation	Indirect Manipulation
Dynamic friction coefficient	0.61	−0.24
Mass	0.53	−0.13
Movement latency	−0.35	0.14
Linear drag coefficient	0.44	−0.12
Angular drag coefficient	0.48	−0.14

subjects' final dynamic friction coefficients. On the other hand, the percent failure for the indirect manipulation of the dynamic friction coefficient task does not show an apparent trend (Fig. 5E). Further, the direct and indirect manipulation results during the MR application with increasing mass values showed similar trends. Fig. 5F portrays the application's first- and third-person viewpoint during both direct and indirect manipulation. Fig. 5G shows the results of the normalized force measurement during direct manipulation. Namely, there is a strong, positive linear trend for increasing mass ($r = 0.53$, $p < 0.001$; Fig. 5G). On the other hand, the indirect manipulation type for the mass MR application does not show a trend ($r = -0.13$, $p > 0.05$; Fig. 5H). Table 3 summarizes the correlation coefficients' results for all the direct and indirect applications.

Similarly, the percent failure for the direct manipulation increases until 40 kg, resulting in all subjects being unable to complete the task for the remaining cubes in the application (Fig. 5I). The corresponding trend of indirect manipulation in the mass application is less consistent. Fig. 5J shows the percent failure of the indirect manipulation with both increasing and decreasing trends. The results of the normalized force measurements and percent failure show that the subjects responded to the effects of increasing physics parameters more strongly and consistently during direct manipulation rather than indirect manipulation. This is supported by the firm positive linear normalized force trend and increasing failure rate for direct manipulation compared to the lack of direction for indirect manipulation. The results of the other three MR applications (i.e., movement latency, linear drag coefficient, and angular drag coefficient) are shown in Figs. S11–S13. These highlight a critical finding related to object manipulation in MR: users augment their pinching force relative to the intensity of the physics parameter and type of manipulation. In rehabilitation, MR provides new perspectives for motor-impaired patients, such as stroke survivors (Duff et al., 2010; Howard and Davis 2022). These novel systems are even potentially more effective than traditional physical therapy methods (Duff et al., 2013). However, current studies have focused on the feasibility of MR rehabilitation and present quantified results through physical ability tests. The findings of this study provide insight into the future development of MR applications with varying physics parameters and manipulation types for rehabilitation. An example of application MR application that could be used for such rehabilitation applications optimized for a patient outcome is portrayed in Fig. S14. Future work should utilize the findings of this study as a foundation for developing rehabilitation-focused MR applications.

4. Conclusion

This paper reports an MR-enabled soft wearable biosensing glove for manipulating various objects with fingers. For the first time, this study shows a quantitative measurement of physical user interactions of object handling and controlling in MR. The soft wearable biosensing system includes a flexible circuit, stretchable interconnectors, a set of soft pressure sensors, and an MR headset, offering a fully portable MR control environment. Our experimental study validates the mechanical and electrical performance of the biosensing glove. Furthermore, our device shows positive, linear relationships with human subjects during the direct manipulation mode between pinching force and dynamic friction coefficient physics parameters. Collectively, the combination of the wearable biosensing system, MR-enabled platform, and capacitive sensors shows potential for various therapeutic program integration, patient rehabilitation tools, and persistent human-machine interfaces.

CRediT authorship contribution statement

Jihoon Kim: Formal analysis, Writing – original draft. **Allison Bayro:** Formal analysis, Writing – original draft. **Jaeho Lee:** Data curation. **Ira Soltis:** Data curation. **Myunghee Kim:** Conceptualization, Writing – review & editing. **Heejin Jeong:** Conceptualization, Funding acquisition, Project administration, Resources, Supervision, Writing – original draft, Writing – review & editing. **Woon-Hong Yeo:** Conceptualization, Formal analysis, Funding acquisition, Project administration, Resources, Supervision, Writing – original draft, Writing – review & editing.

Declaration of competing interest

The authors declare the following financial interests/personal relationships which may be considered as potential competing interests: Georgia Tech has a pending US patent application.

Data availability

Data will be made available on request.

Acknowledgements

We acknowledge the support of the National Science Foundation/the Centers for Disease Control and Prevention (grant NRI-2024742). This study was partially supported by the IEN Center Grant from the Georgia Tech Institute for Electronics and Nanotechnology. Wearable devices in this work were fabricated at the Institute for Electronics and Nanotechnology, a member of the National Nanotechnology Coordinated Infrastructure, which is supported by the National Science Foundation (grant ECCS-2025462).

Appendix A. Supplementary data

Supplementary data to this article can be found online at https://doi.org/10.1016/j.biosx.2023.100343.

References

Alexandre, R., Postolache, O., Girão, P.S., 2019. Physical rehabilitation based on smart wearable and virtual reality serious game. In: 2019 IEEE International Instrumentation and Measurement Technology Conference (I2MTC). IEEE, pp. 1–6.
Almeida, L., Lopes, E., Yalçinkaya, B., Martins, R., Lopes, A., Menezes, P., Pires, G., 2019. Towards Natural Interaction in Immersive Reality with a Cyber-Glove. 2019 IEEE International Conference on Systems, Man and Cybernetics (SMC). IEEE, pp. 2653–2658.
Anderson, K.E., Gruber-Baldini, A.L., Vaughan, C.G., Reich, S.G., Fishman, P.S., Weiner, W.J., Shulman, L.M., 2007. Impact of psychogenic movement disorders versus Parkinson's on disability, quality of life, and psychopathology. Mov. Disord.: off. j. Mov. Disord. Soc. 22 (15), 2204–2209.
Bannach, D., Amft, O., Kunze, K.S., Heinz, E.A., Troster, G., Lukowicz, P., 2007. Waving real hand gestures recorded by wearable motion sensors to a virtual car and driver in a mixed-reality parking game. In: 2007 IEEE Symposium on Computational Intelligence and Games. IEEE, pp. 32–39.
Brocklehurst, J.C., Morris, P., Andrews, K., Richards, B., Laycock, P., 1981. Social effects of stroke. Soc. Sci. Med. Med. Psychol. Med. Sociol. 15 (1), 35–39.
Cappello, L., Meyer, J.T., Galloway, K.C., Peisner, J.D., Granberry, R., Wagner, D.A., Engelhardt, S., Paganoni, S., Walsh, C.J., 2018. Assisting hand function after spinal cord injury with a fabric-based soft robotic glove. J. NeuroEng. Rehabil. 15 (1), 1–10.
Cha, Y., Seo, J., Kim, J.-S., Park, J.-M., 2017. Human–computer interface glove using flexible piezoelectric sensors. Smart Mater. Struct. 26 (5), 057002.
Duff, M., Chen, Y., Attygalle, S., Herman, J., Sundaram, H., Qian, G., He, J., Rikakis, T., 2010. An adaptive mixed reality training system for stroke rehabilitation. IEEE Trans. Neural Syst. Rehabil. Eng. 18 (5), 531–541.

Duff, M., Chen, Y., Cheng, L., Liu, S.-M., Blake, P., Wolf, S.L., Rikakis, T., 2013. Adaptive mixed reality rehabilitation improves quality of reaching movements more than traditional reaching therapy following stroke. Neurorehabilitation Neural Repair 27 (4), 306–315.

Dwivedi, A., Kwon, Y., Liarokapis, M., 2020. Emg-based decoding of manipulation motions in virtual reality: towards immersive interfaces. In: 2020 IEEE International Conference on Systems, Man, and Cybernetics (SMC). IEEE, pp. 3296–3303.

Feigin, V.L., Vos, T., Nichols, E., Owolabi, M.O., Carroll, W.M., Dichgans, M., Deuschl, G., Parmar, P., Brainin, M., Murray, C., 2020. The global burden of neurological disorders: translating evidence into policy. Lancet Neurol. 19 (3), 255–265.

Gailey, A.S., Godfrey, S.B., Breighner, R.E., Andrews, K.L., Zhao, K.D., Bicchi, A., Santello, M., 2017. Grasp performance of a soft synergy-based prosthetic hand: a pilot study. IEEE Trans. Neural Syst. Rehabil. Eng. 25 (12), 2407–2417.

Hamacher, A., Kim, S.J., Cho, S.T., Pardeshi, S., Lee, S.H., Eun, S.-J., Whangbo, T.K., 2016. Application of virtual, augmented, and mixed reality to urology. Int. Neurourol. J. 20 (3), 172.

Howard, M.C., Davis, M.M., 2022. A meta-analysis and systematic literature review of mixed reality rehabilitation programs: investigating design characteristics of augmented reality and augmented virtuality. Comput. Hum. Behav., 107197

Jeong, H., Bayro, A., Umesh, S.P., Mamgain, K., Lee, M., 2022. Social media users' perceptions of a wearable mixed reality headset during the COVID-19 pandemic: aspect-based sentiment analysis. JMIR Ser. Games 10 (3), e36850.

Jiang, X., Xiao, Z.G., Menon, C., 2018. Virtual grasps recognition using fusion of Leap Motion and force myography. Virtual Real. 22 (4), 297–308.

Kim, D., Park, K., Lee, G., 2021. Atatouch: robust finger pinch detection for a vr controller using rf return loss. In: Proceedings of the 2021 CHI Conference on Human Factors in Computing Systems, pp. 1–9.

Lopes, P., You, S., Ion, A., Baudisch, P., 2018. Adding force feedback to mixed reality experiences and games using electrical muscle stimulation. In: Proceedings of the 2018 Chi Conference on Human Factors in Computing Systems, pp. 1–13.

Lünenburger, L., Colombo, G., Riener, R., 2007. Biofeedback for robotic gait rehabilitation. J. NeuroEng. Rehabil. 4 (1), 1–11.

Muangpoon, T., Osgouei, R.H., Escobar-Castillejos, D., Kontovounisios, C., Bello, F., 2020. Augmented reality system for digital rectal examination training and assessment: system validation. J. Med. Internet Res. 22 (8), e18637.

Mukaka, M.M., 2012. A guide to appropriate use of correlation coefficient in medical research. Malawi Med. J. 24 (3), 69–71.

Radwin, R.G., Oh, S., Jensen, T.R., Webster, J.G., 1992. External finger forces in submaximal five-finger static pinch prehension. Ergonomics 35 (3), 275–288.

Shi, B., Chen, X., Yue, Z., Yin, S., Weng, Q., Zhang, X., Wang, J., Wen, W., 2019. Wearable ankle robots in post-stroke rehabilitation of gait: a systematic review. Front. Neurorob. 13, 63.

Spain, R., Bailey, S.K., Goldberg, B., Sail, R., Carmody, K., Ficke, C., Bayro, A., Jeong, H., Kim, J., Hong Yeo, W., 2022. Me and my VE 2022: human factors applications using virtual reality, mixed reality, and virtual environments. In: Proceedings of the Human Factors and Ergonomics Society Annual Meeting. SAGE Publications Sage CA, Los Angeles, CA, pp. 2188–2192.

Tsai, Y.-T., Jhu, W.-Y., Chen, C.-C., Kao, C.-H., Chen, C.-Y., 2021. Unity game engine: interactive software design using digital glove for virtual reality baseball pitch training. Microsyst. Technol. 27 (4), 1401–1417.

Wu, Y.-T., Chen, K.-H., Ban, S.-L., Tung, K.-Y., Chen, L.-R., 2019. Evaluation of leap motion control for hand rehabilitation in burn patients: an experience in the dust explosion disaster in Formosa Fun Coast. Burns 45 (1), 157–164.